Droplet size and velocity measurements at the outlet of a hollowcone spray nozzle

Arnaud Foissac, Jeanne Malet, Maria Rosaria Vetrano, Jean-Marie Buchlin, Stephane Mimouni, Francois Feuillebois, Olivier Simonin

Atomization and Sprays, 21 (11): 893–905 (2011)

DROPLET SIZE AND VELOCITY MEASUREMENTS AT THE OUTLET OF A HOLLOW CONE SPRAY NOZZLE

Arnaud Foissac,[1,*] Jeanne Malet,[1] Maria Rosaria Vetrano,[2] Jean-Marie Buchlin,[2] Stéphane Mimouni,[3] François Feuillebois,[4] & Olivier Simonin[5]

[1] *IRSN, DSU/SERAC/LEMAC, BP 68, F-91192 Gif-sur-Yvette Cedex, France*

[2] *VKI, Chaussée de Waterloo, 7, B-1640 Rhode-St-Genèse, Belgium*

[3] *EDF R&D, MFEE, 6 quai Watier, F-78400 Chatou, France*

[4] *LIMSI-CNRS, BP 133, F-91403 Orsay Cedex, France*

[5] *IMFT, 1 allée du Professor Camille Soula, F-31000 Toulouse, France*

[*] Address all correspondence to Arnaud Foissac E-mail: arnaud.foissac@irsn.fr

Original Manuscript Submitted: 10/12/2011; Final Draft Received: 3/5/2012

During the course of a severe accident in a nuclear pressurized water reactor (PWR), hydrogen may be produced by reactor core oxidation and distributed into the containment. Spray systems are used in order to limit overpressure, enhance the gas mixing, avoid hydrogen accumulation, and wash out fission products. In order to simulate these phenomena with computational fluid dynamics codes, it is first necessary to know the droplet size and velocity distributions close to the outlet nozzle. Furthermore, since most of the phenomena relative to droplets (condensation, gas entrainment, and collisions) are of particular importance in the region just below the nozzle, accurate input data are needed for real-scale PWR calculations. The objective is, therefore, to determine experimentally these input data under atmospheric conditions. Experimental measurements were performed on a single spray nozzle, which is routinely set up in many PWRs. This nozzle is generally used with water at a relative pressure supply of 3.5 bar, producing a mass flow rate of approximately 1 kg/s. At a distance of 20 cm, in which under ambient conditions atomization is just achieved, it is found that the geometric mean diameter varies from 280 to 340 μm, the Sauter mean diameter varies from 430 to 520 μm, and the mean axial velocity varies from 14 to 20 m/s. The radial velocity is around 7 m/s, whereas the orthoradial velocity is almost equal to zero at this distance of the nozzle. Gas velocity measurements around the spray are also performed.

KEY WORDS: *spray, phase-Doppler anemometer, droplet size distribution, droplet velocity distribution, air entrainment, CFD numerical input data*

1. INTRODUCTION

One of the main contributors to early failure in containment during a pressurized water reactor (PWR) severe accident is associated with the presence of hydrogen within the containment building. The hydrogen produced by reactor core oxidation and released from the reactor coolant system could mix or accumulate in different parts of the containment. If the composition of the hydrogen–steam–air mixture

reaches a certain threshold, combustion could occur. In order to prevent such a risk, an array of spray nozzle systems is positioned at the top of the containment. These sprays are used to limit overpressure, enhance the gas mixing, avoid hydrogen accumulation, and wash out fission products and structure materials that may be released. The spray system efficiency may depend on the evolution of the droplet sizes and velocity distributions during their fall, especially in the region just below the spray nozzle where most droplet phenomena occur; i.e., condensation (Mimouni et al., 2008), gas entrainment (Cossali, 2001), and collisions (Qian and Law, 1997; Rabe et al., 2009).

Some of the nozzles usually used in spray systems in many PWRs have already been characterized by Powers and Burson (1993), who used photographic and freezing methods, and by Ducret et al. (1993), who used a micro-video system. These works give interesting information about the spray nozzle characterization but, unfortunately, no information is given about the location where the measurements were performed. Recent developments of computational fluid dynamics (CFD) codes as well as experimental techniques involving laser diagnostics offer the possibility to more accurately characterize actual PWR spray systems. Thus, the objective of this work is to provide the first detailed characterization of the PWR spray nozzle in three dimensions, in terms of spray shape, droplet size, and three-dimensional (3D) droplet velocity distributions at spray locations as close as possible to the nozzle outlet. Such measurements will give accurate and detailed boundary conditions for CFD numerical simulations of spray behavior. This set of data provides a valuable improvement, since appropriate boundary conditions are mandatory for relevant CFD calculations. Moreover, since the internal geometry of the PWR nozzle is known and available from the distributor Lechler (http://www.lechlerusa.com/), it is possible to simulate accurately the liquid flow. Therefore, knowing the characteristics of the droplets at the outlet of the nozzle can be interesting to validate atomization models.

2. PWR CONTAINMENT SPRAY SYSTEMS

Spray systems are emergency devices designed for preserving the containment integrity in case of a severe accident in a PWR. The French PWR containment buildings generally have two series of nozzles placed in circular rows (Coppolani et al., 2004). More precisely, for the 900 MWe PWR, there are exactly four rings of nozzles, the characteristics of which are presented in Table 1. Schematic views of these spray rings and the associated spray envelopes are given in Fig. 1.

The nozzle type used in many PWRs, in particularly French 900 MWe PWRs, is the so-called SPRACO 1713A, distributed by Lechler under Reference No. 373.084.17.BN (Fig. 2). This nozzle is generally used with water at a relative pressure of 3.5 bar, producing a flow rate of approximately 1 L/s. The outlet orifice diameter is 9.5 mm. The temperature of the injected water during a hypothetical nuclear reactor accident is either 20°C or from 60 to 100°C, depending on the kind of process (the 60 to 100°C process is the so-called recirculation mode).

Powers and Burson (1993) and Ducret et al. (1993) gave droplet size distributions for this nozzle. However, they did not precisely identify the location at which the measurements of the spray were

TABLE 1: Characteristics of spray rings for the French 900 MWe PWR

Spray ring	Height (m)	Diameter (m)	Number of nozzles	Estimated minimum distance between nozzles (m)
First ring	54.8	10.0	66	0.5
Second ring	54.2	14.8	68	0.7
Third ring	52.3	22.5	186	0.4
Fourth ring	51.0	27.0	186	0.4

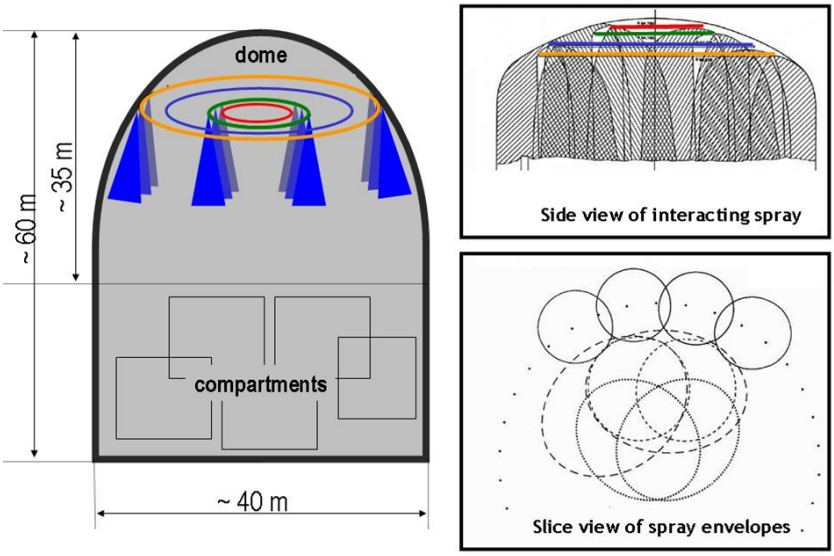

FIG. 1: Spray rings and envelopes in a French PWR (not to scale).

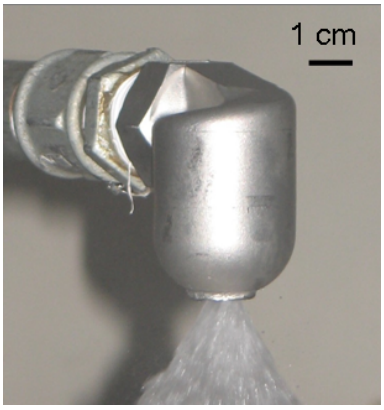

FIG. 2: Spray nozzle SPRACO 1713A (Lechler 373.084.17.BN).

performed. Nowadays, more information can be obtained using methods such as phase-Doppler interferometer (PDI), diffractometry, or shadowgraphy. Furthermore, the PDI technique allows the determination of the spatial distribution of the droplet size together with the velocity close to the nozzle outlet.

3. EXPERIMENTAL FACILITY

The experiments were carried out at the French Institute for Radiological Protection and Nuclear Safety (IRSN), in the Characterization and Application of Large and Industrial Spray Transfer (CALIST) Facility (see Fig. 3), which was inspired by the facility available at the von Karman Institute, where global spray characterization was first performed. However, the von Karman Institute facility is too small to perform measurements in all the parts of the spray. Moreover, this facility could not be easily adapted to the measurement of the gas velocity. The setup is composed of a hydraulic circuit supplying, for those experiments, a single spray nozzle with a flow rate of 1 L/s at a relative pressure of 3.5 bar. The pulverized water is collected in a 5 m^3 pool. The axial position

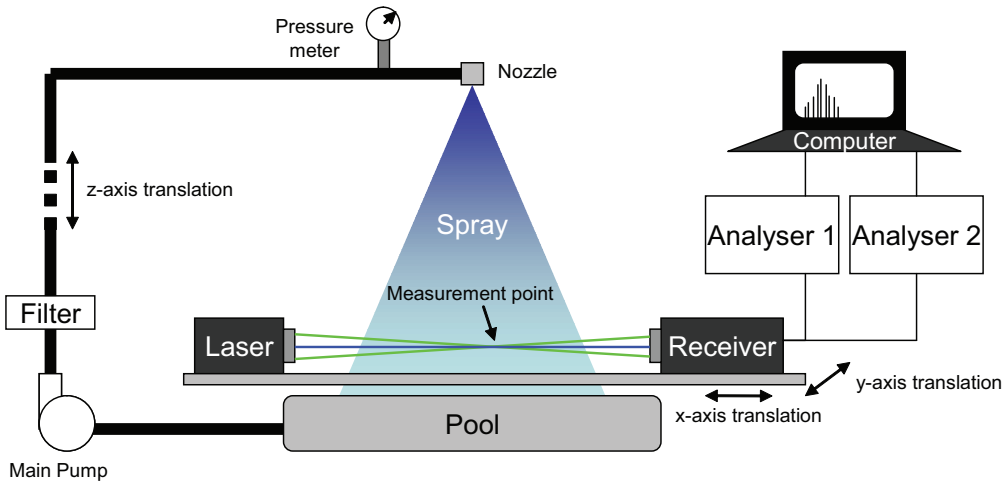

FIG. 3: CALIST water-spray experimental facility.

of the spray nozzle can be changed using a monitored carriage.

The measurement of the spray characteristics requires a technique such as the light diffraction, shadowgraphy, or PDI. The latter was chosen since it provides high-resolution local information about the spray drops. Indeed, PDI measures the size and velocity of drops passing through an optically defined probe volume (Bachalo and Houser, 1984). The laser light sources of the present two-dimensional (2D) Artium PDI system (http://www.artium.com/) are two solid-state continuous-wave laser systems, a blue one with a wave length at 473 nm and a green one with a wave length at 532 nm. The off-axis angle (scattering angle), at which the receiving optics unit is placed, is 30°. Lenses of 2 m focal length have been used so that diameters from 20 to 2000 μm could be detected.

PDI can only measure droplets of spherical shape. In order to determine where atomization is achieved (i.e., where droplets are spherical), visualization was performed with a Phantom high-speed camera (http://www.visionresearch.com/) used with a resolution of 800×600 pixels at a frequency of 4796 Hz, with an exposure time of 10 μs. The spray close to the nozzle outlet, where atomization occurs, was illuminated from the back in order to obtain consistent and machine readable images. All measurements were performed in air under atmospheric conditions (ambient pressure of 1 bar and ambient temperature of 20°C).

Even if these experimental conditions (pressure, temperature, and gaseous composition) are not similar to the ones of a PWR containment in a situation of a severe accident, it is important to note that these results on this nozzle are the first ever found.

4. EXPERIMENTAL RESULTS

4.1 Global Spray Characterization

4.1.1 Characteristic Numbers

Experimental measurements were performed with supply water under relative pressures of 3.5, 5, and 7 bar. The measured flow rate, flow number FN, and discharge coefficient C_D were measured and are presented in Table 2. The flow number denotes the effective flow area of the exit orifice and is calculated from the mass flow rate and injection pressure as follows:

$$\mathrm{FN} = \frac{Q_m}{\sqrt{\Delta P}} \tag{1}$$

where Q_m is the mass flow rate (kg/s) and ΔP is the relative pressure between the nozzle and the outlet.

The following discharge coefficient is used to describe the behavior of a nozzle:

TABLE 2: Values of flow rate, flow number, and discharge coefficient of the SPRACO 1713A nozzle for relative water supply pressures from 3.5 to 7 bar

Relative pressure (bar)	Flow rate (L/s)	Flow number (kg/s^{-1}Pa$^{-0.5}$)	Discharge coefficient
3.5	1.04	0.00176	0.55
5	1.22	0.00173	0.54
7	1.50	0.00179	0.56

$$C_D = \frac{Q_V}{S\sqrt{2\Delta P/\rho_l}} \tag{2}$$

Here, Q_v is the volumetric flow rate (m^3/s), S is the surface of the nozzle outlet, and ρ_l is the density of the liquid injected. The value of this coefficient depends on the pressure drop, as well as on the turbulent energy and the presence of a secondary flow. If C_D equals unity, the whole energy is transferred to the flow at the nozzle outlet.

The flow number appears to be constant by increasing the pressure. Therefore, this nozzle follows classic behavior (Lefebvre, 1989). The values of the discharge coefficient showed that almost half of the energy was lost in the nozzle, regardless of the value of the pressure.

4.1.2 Atomization

A spray is usually created by the instability of either a liquid jet or sheet at the outcome of the nozzle (Dumouchel, 2008). When surface forces become weaker than inertial forces, atomization occurs; i.e., the liquid jet/sheet breaks into filaments that shatter into droplets. The high-speed visualization showed that the distance from the nozzle exit at which most of the liquid was atomized into droplets was approximately 20 cm, as depicted in Fig. 4. Before 20 cm, the spray was too dense and the validation rate of the PDI was too low. Therefore, it may be anticipated that PDI measurements of droplets are reliable from 20 cm (Fig. 5). The relative water supply pressure was fixed at 3.5 bar for all results presented in the following sections.

4.2 Local Water Concentration

In agreement with information provided by the nozzle manufacturer, it was found that the SPRACO 1713A nozzle creates a hollow cone spray (Fig. 6). The spray angle was found to be around 60° (Fig. 5). Only a few droplets of very small diameter (less than 100 μm) were present in the core of the spray. At a distance of 20 cm from the nozzle, due to the hollow cone created by this nozzle, most of the droplets were concentrated in an annular area situated between 8 and 15 cm from the nozzle axis, with a maximum

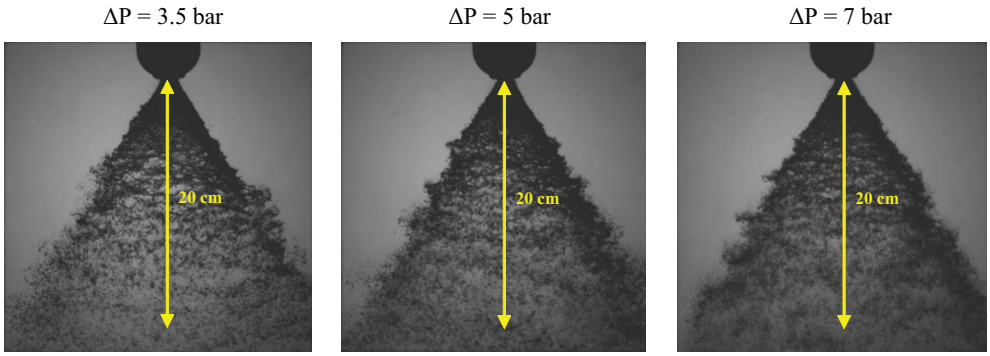

FIG. 4: High-speed camera images of the SPRACO 1713A nozzle at relative water supply pressures of 3.5, 5, and 7 bar.

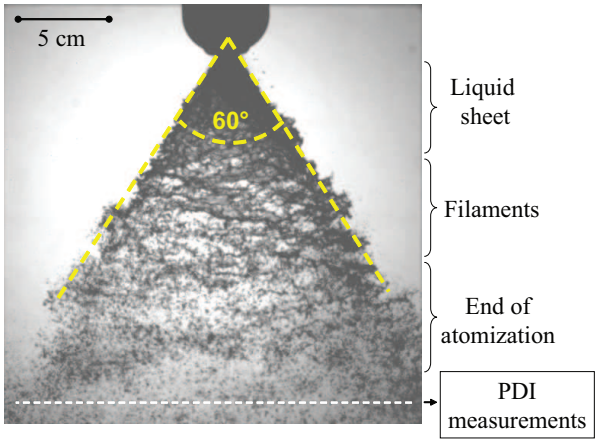

FIG. 5: Position of reliable PDI measurements of sprays produced by the SPRACO 1713A nozzle at a relative water supply pressure of 3.5 bar.

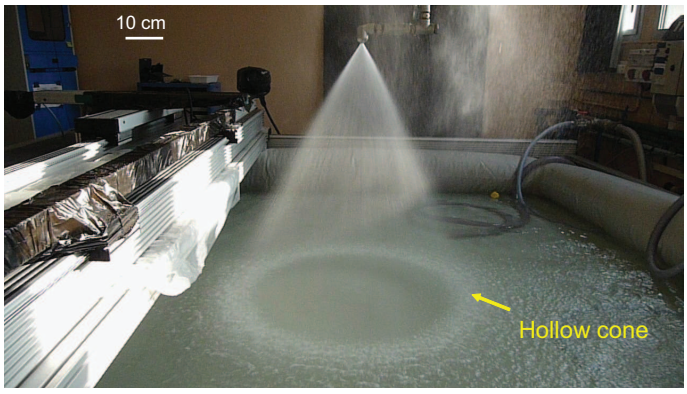

FIG. 6: Annular cross section of the hollow cone spray.

presence at 11 cm, as seen in Fig. 7. This local water concentration (kg/m^3) was measured with the PDI. Here, this technique provides good approximate data, even though it is known not to be the best one for evaluating liquid concentrations.

4.3 Description of the Measurement Points

PDI measurements of droplet size and velocity distributions were performed at 20 cm from the nozzle outlet. Four measurement series, separated by 90° angles, were performed at six radial positions situated in the annular area described in Fig. 8.

The spray stability was tested during a 30 min PDI measurement. This result was compared to 20 measurements of 30 s. Between each of them, the pump was stopped and restarted. Figure 9 shows that the droplet size and velocity measurement of the spray characteristics were stable. In the set of the 20 measurements of 30 s each, the geometric mean diameter D_{10} varied from 311 to 313 μm (standard deviation of 1.3 μm), the Sauter mean diameter D_{32} varied from 510 to 523 μm (standard deviation of 6.3 μm), the droplet mean axial velocity varied from 15.68 to 15.76 m/s (standard deviation of 0.04 m/s), and the droplet mean radial velocity varied from 7.69 to 7.88 m/s (standard deviation of 0.1 m/s).

In the following, mean data from PDI measurements will be presented for each spray radius R, by averaging over all azimuthal angles (from 0° to

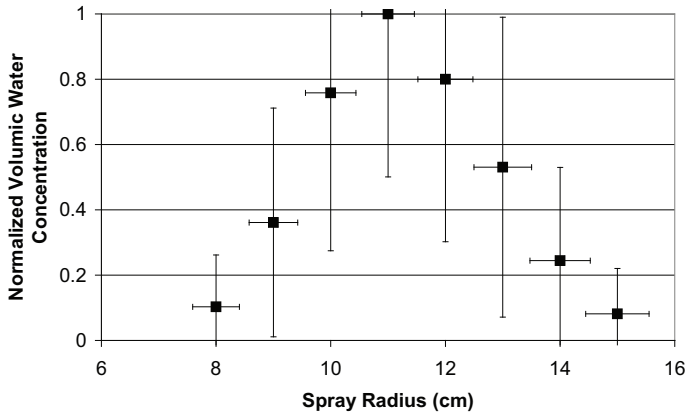

FIG. 7: Normalized local water concentration at 20 cm from the nozzle outlet as a function of distance from the nozzle axis. The relative water supply pressure is 3.5 bar.

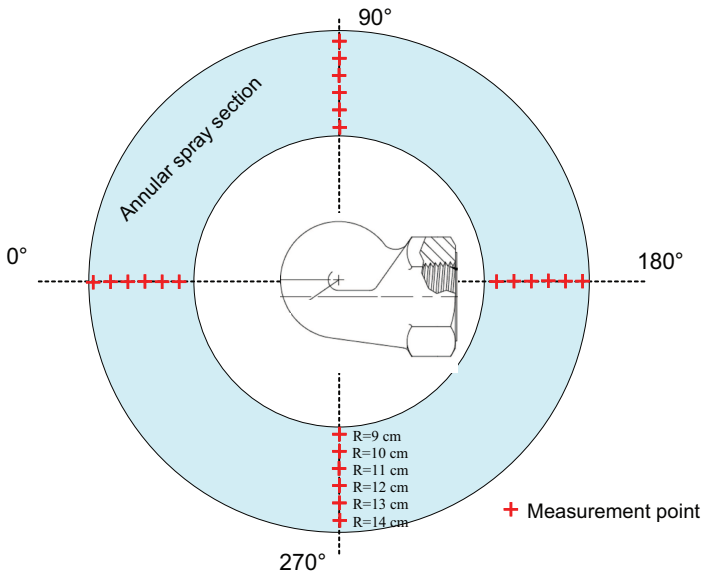

FIG. 8: Position of the measurement points in the cross section of the hollow cone spray (top view).

270°). The standard deviation over azimuthal angles will confirm the hypothesis of cylindrical symmetry of the spray.

Since the spray was slightly pulsating at 3.5 bar at 20 cm from the nozzle orifice, it was estimated that the spray angle α uncertainty was $\sigma_\alpha = \pm 1°$. Hence, the uncertainty σ_R on the measurement position (Fig. 10) is:

$$\sigma_R = 20 \tan\left(\tan^{-1}\frac{R}{20} + \sigma_\alpha\right) - R \qquad (3)$$

This uncertainty σ_R led to an uncertainty σ_Y on the measured value Y. Indeed, if the measurement was performed in an area where Y varied strongly, the uncertainty σ_Y became important. It was, therefore, calculated from the evolution of Y when the spray radius R varied with σ_R (Fig. 11).

Finally, for each measurement point, the droplet size and axial velocity distributions were measured three times. In the following figures (Figs. 13, 15, and 18), the error bars are estimated from the differences

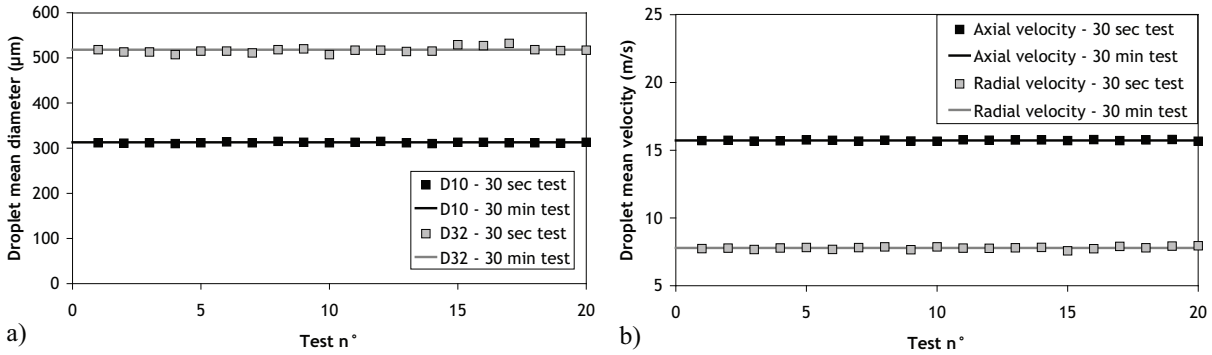

FIG. 9: Study of the measurement stability comparing a 30-min test to 30-s tests at the same position in the spray: (a) droplet geometric mean D_{10} and Sauter mean D_{32} diameters; (b) droplet axial and radial velocities.

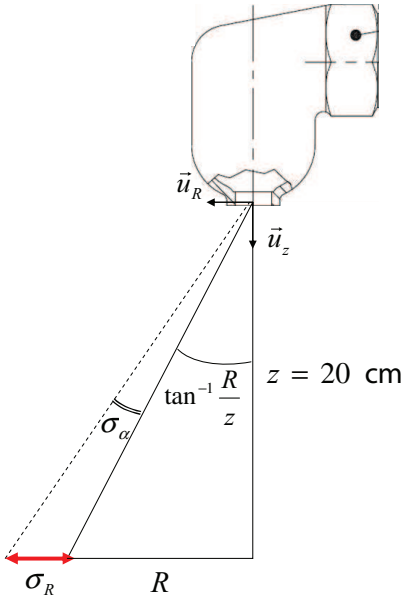

FIG. 10: Estimation of the uncertainty σ_R of the measurement position due to the spray pulse phenomenon involving an uncertainty of 1° on the spray angle value.

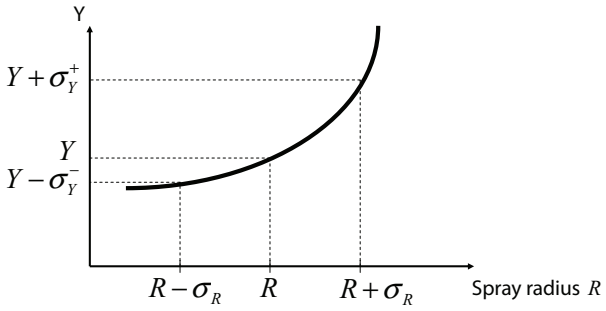

FIG. 11: Estimation of the uncertainty σ_Y associated with the measurement position uncertainty σ_R.

between these three tests for each position and from the uncertainties presented above.

4.4 Drop Size Distribution

Size distributions, measured at a distance of 20 cm from the nozzle outlet, and at various radial positions, are presented in Fig. 12. They are normalized by their maximum value. These data are averages of the three size distributions obtained during the three series of measurements. The size distributions obtained by the average of the three measurements, for all radial distances, can be well fitted, for all the spray radii, by a log-normal law with a standard deviation σ of 0.5 and a mean diameter d_{mean} of 260 μm, as plotted in Fig. 12:

$$f(d) = \frac{1}{\sqrt{2\pi}\sigma\, d} \exp\left(-\frac{[\ln(d) - \ln(d_{\text{mean}})]^2}{2\sigma^2}\right)$$
$$\sigma = 0.5 \quad \text{and} \quad d_{\text{mean}} = 260\ \mu\text{m} \tag{4}$$

For each measured size distribution, global spray features (i.e., geometric mean diameter D_{10} and Sauter mean diameter D_{32}) were calculated. The results are displayed in Fig. 13. The mean diameter D_{10} changed slightly with the radial position, from around 280 to 340 μm, and the Sauter mean diameter changed from around 430 to 520 μm. The smallest droplets were

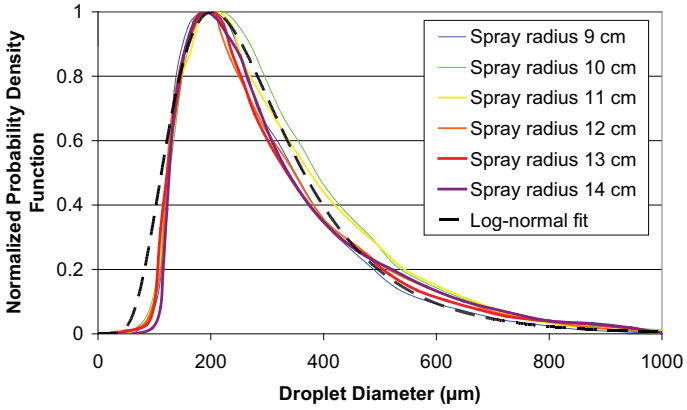

FIG. 12: Experimental averaged droplet size distributions at 20 cm from the nozzle outlet at various radial positions from 9 to 14 cm, normalized by the maximum value.

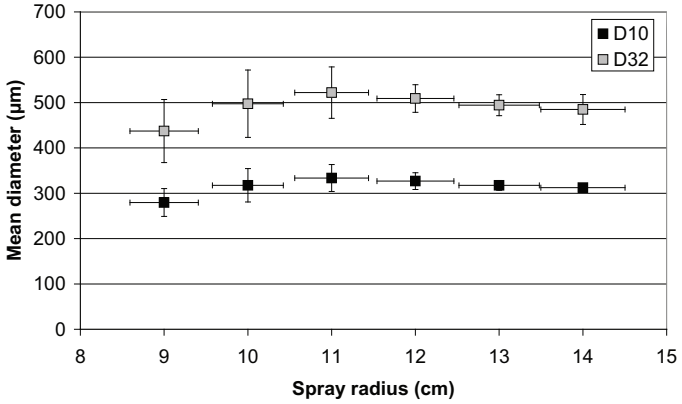

FIG. 13: Geometric mean diameter D_{10} and Sauter mean diameter D_{32} at 20 cm from the nozzle outlet as a function of the radial distance in the spray.

observed at low radial distances. This may be explained by the entrainment of droplets by air, since small droplets are much more sensitive to the drag force than the biggest ones. This is due to an air flow that is created by the spray in the direction of the center of the spray (Cossali 2001) and the small droplets tend to follow this direction.

4.5 Velocity Distribution

Measurements of the droplet velocity were also performed at a distance of 20 cm from the nozzle orifice. The droplet axial velocity distributions, normalized by their maximum value, are plotted in Fig. 14. Their shape is rather similar for all positions on the annular ring of the spray envelope, even though the mean values differ.

The radial and orthoradial velocity distributions cannot be directly measured with this experimental setup. PDI measurements were performed in the *x*-*y* plane, so that V_x and V_y could be measured. The angle between the radial velocity V_r and the *y* axis and the one between the orthoradial velocity V_θ and the *x* axis were known, since it is a characteristic of our setup. Its value is 15°. Therefore, V_r was given by $V_r = V_y/\cos 15^\circ$ and V_θ was given by $V_\theta = V_x/\cos 15^\circ$.

These polar components of velocity, together with the mean droplet axial velocity, are plotted in Fig. 15. The mean axial velocity decreased from 20 to 14 m/s, whereas the radial velocity increased from 5.8 to 7.4

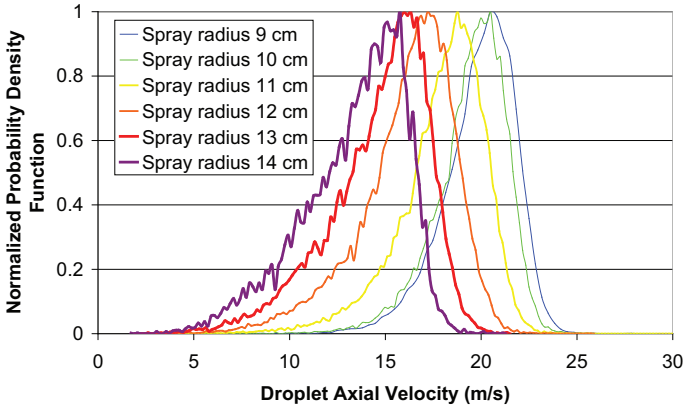

FIG. 14: Droplet axial velocity at 20 cm from the nozzle outlet at various radial positions from 9 to 14 cm, normalized by the maximum value.

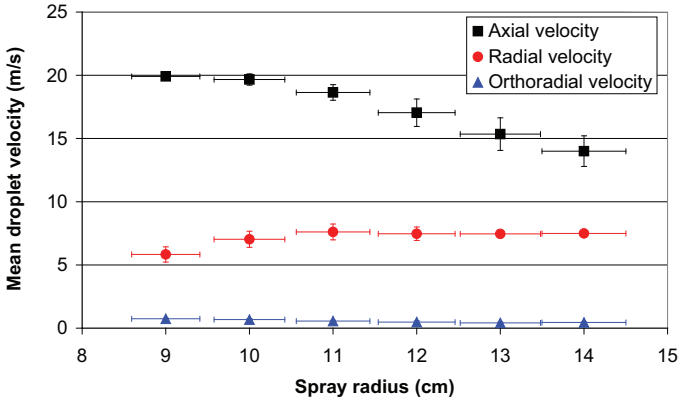

FIG. 15: Mean value of the axial, radial, and orthoradial droplet velocities at 20 cm from the nozzle outlet as a function of the radial distance in the spray.

m/s. The orthoradial velocity can be neglected since its maximum value is 0.3 m/s.

4.6 Velocity–Size Correlation

To perform velocity–size correlations, the droplet population was divided into classes on the basis of their diameters. These classes were 50 μm in width and, using the measurements performed on the spray, we obtained the axial velocity distribution for each group of droplets. We then derived the velocity–size correlation. Indeed, small droplets do not have the same velocity as bigger ones, mainly due to the drag force. Knowing the actual velocity of each droplet size is useful for data input in numerical simulations. In particular, these experimental data can be directly used in the sectional approach (Greenberg et al., 1993) or the multifluid method (Laurent and Massot, 2001; Fox et al., 2008).

The mean results are given for different spray radial positions at a distance of 20 cm from the nozzle outlet (Fig. 16). Even if the experimental setup cannot provide the same type of results for the radial velocity, the radial velocity–size correlation can be evaluated. Considering that, for a given spray radius, trajectories of droplets are independent on their diameter, the radial velocity may then be calculated from the axial velocity–size correlation. The results are plotted in Fig. 17. It can be noticed that mean axial velocity increases with the diameter. A plateau

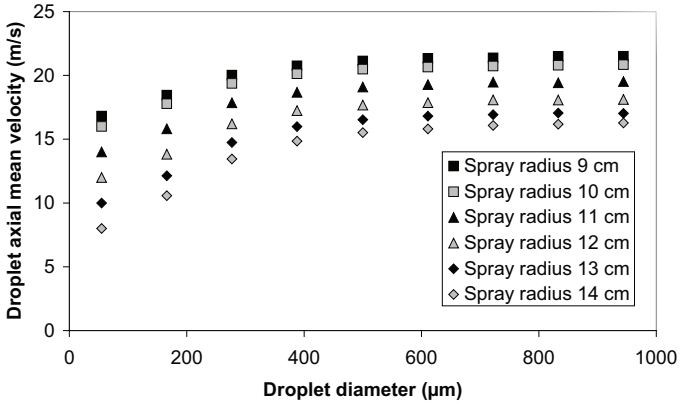

FIG. 16: Mean axial velocity-size correlation at 20 cm from the nozzle outlet at various radial positions from 9 to 14 cm.

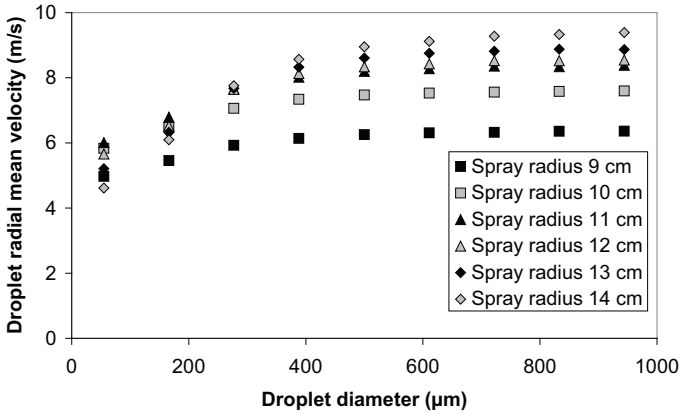

FIG. 17: Mean radial velocity-size correlation at 20 cm from the nozzle outlet at various radial positions from 9 to 14 cm.

of mean velocity seems to be reached for droplets with diameters higher than 300 μm. Under this limit, the Stokes number becomes close to unity, which means that these droplets can be influenced by the gas around them.

5. GAS VELOCITY AROUND THE SPRAY

A gas flow is created by the spray due to the drag force between the gas and the droplets (Cossali, 2001). The experimental setup at the CALIST facility allows estimating the gas velocity. For that purpose, fog nozzles producing small droplets of 50 μm were fixed at the top of the CALIST. Without the PWR spray, the velocity of these droplets, at the place where the measurement was performed, was equal to approximately 0.6 m/s. By comparison with their diameter, the terminal fall velocity of the fog droplets was about 0.3 m/s. The Stokes number of fog droplets, using a characteristic length scale of 0.1 m, which corresponds to the radius of curvature of the gas trajectory observed experimentally, and a characteristic velocity of 1 m/s, estimated from the PDI measurements (Fig. 18), was of the order of 7×10^{-2}, which is small compared with unity. This means that droplets adapt fast to the change in the ambient flow field. Thus, characteristic values of this flow field may be estimated with the fog droplet motion. Figure 18 gives the axial and radial mean velocity of the 50 μm fog droplets when the PWR spray was activated.

6. CONCLUSION

Measurements of the hydrodynamic characteristics of a real-scale spray nozzle (SPRACO 1713A) currently used in PWRs, have been performed for the first time in terms of droplet size and axial velocity distributions. Measurements have been conducted as close as possible to the nozzle outlet (i.e., at 20 cm from the nozzle orifice), where the atomization process appears to be completed, as observed experimentally with a high-speed camera. Droplet size and velocity distribution have been obtained for typical conditions used in nuclear reactors (i.e., a relative pressure supply of 3.5 bar).

However, in a nuclear containment during a severe accident, pressure and temperature in the containment can increase. Therefore, the physical properties of the gas and liquid are different from the ones used in this experiment, and this could lead to changes in the size and velocity distributions. Further work is necessary to estimate these changes, but due to the size of the spray produced, experiments with high pressure and high temperature are difficult to perform, especially because it is important to keep free space around the spray to avoid wall influence.

These results give a full overview of the spray characteristics and can be directly used as input data for CFD calculations of real-scale sprays in nuclear reactors. It should be emphasized that the considered spray region is of particular importance since most

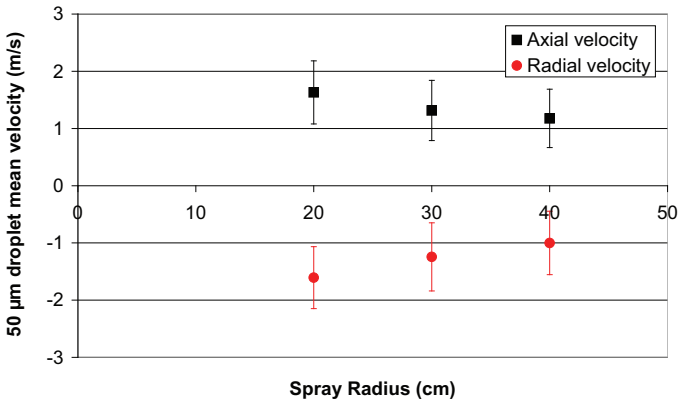

FIG. 18: The 50 μm droplet mean axial and radial velocities at 20 cm from the nozzle outlet as a function of the radial distance in the spray.

of the phenomena relative to droplets (condensation, gas entrainment, and collisions) are enhanced in the region below the spray nozzle. Finally, these data can be used to validate atomization models on spray with the importance of size, the works of which are still quite poor in the available literature.

REFERENCES

Bachalo, W. D. and Houser, M. J., Phase/Doppler spray analyzer for simultaneous measurements of drop size and velocity distributions, *Opt. Eng.*, vol. **23**, pp. 583–590, 1984.

Coppolani, P., Hassenboehler, N., Joseph, J., Petetrot, J.-F., Py, J.-P., and Zampa, J.-S., *La Chaudière des Réacteurs à Eau sous Pression*, Les Ulis, France: EDP Science, 2004.

Cossali, G. E., An integral model for gas entrainment into full cone sprays, *J. Fluid Mech.*, vol. **439**, pp. 353–366, 2001.

Ducret, D., Vendel, J., and Vigla, D., Etude préliminaire de l'aspersion, *IRSN Technical Report IPSN/DSU/SERAC/LECEV93/22*, 1993.

Dumouchel, C., On the experimental investigation on primary atomization of liquid streams, *Exp. Fluids*, vol. **45**, pp. 371–422, 2008.

Fox, R. O., Laurent, F., and Massot, M., Numerical simulation of spray coalescence in an Eulerian framework: Direct quadrature method of moments and multi-fluid method, *J. Comput. Phys.*, vol. **227**, pp. 3058–3088, 2008.

Greenberg, J. B., Silverman, I., and Tambour, Y., On the origin of spray sectional conservation equations, *Combust. Flame*, vol. **93**, pp. 90–96, 1993.

Laurent, F. and Massot, M., Multi-fluid modelling of laminar polydisperse spray flames: Origin, assumptions and comparison of sectional and sampling methods, *Combust. Theor. Model.*, vol. **5**, pp. 537–572, 2001.

Lefebvre, A. H., *Atomization and Sprays*, New York: Taylor & Francis, 1989.

Mimouni, S., Lamy, J.-S., and Lavieville, J., Modelling of sprays in containment applications with a CMFD code, *Proc. of XCFD4NRS Conference*, Grenoble, France, 2008.

Powers, D. A. and Burson, S. B., A simplified model of aerosol removal by containment sprays, *Report NUREG/CR-5966*, Washington, DC: Nuclear Regulatory Commission, 1993.

Qian, J. and Law, C. K., Regimes of coalescence and separation in droplet collision, *J. Fluid Mech.*, vol. **331**, pp. 59–80, 1997.

Rabe, C., Malet, J. and Feuillebois, F., On the influence of droplet coalescence in spray systems for containment safety, *Proc. of 13th International Topical Meeting on Nuclear Reactor Thermal Hydraulics Conference*, Kanazawa City, Japan, 2009.